

JET PROPULSION LABORATORY
CALIFORNIA INSTITUTE OF TECHNOLOGY
PASADENA, CALIFORNIA

Transfer of Copyright

The contribution entitled "Benefits of **Model** Updating: A Case Study Using the Micro-precision Interferometer Testbed" by San-jay S. Joshi, James W. Melody, **Gregory** W. Neat, and Andrew **Kissil** scheduled for publication 'i-n the-Proceedings of DETC '97 has been cleared for public release by the Jet 'Propulsion Laboratory, California Institute of Technology, and copyright to that contribution is hereby transferred to the American Society of Mechanical Engineers effective if and when the contribution is published by the above named publisher.

This contribution is a work made for hire, and in accordance with the contract between the California Institute of Technology and the National Aeronautics and Space Administration, the United States Government, and others acting on its behalf, shall have, for Governmental purposes, a royalty-free, nonexclusive, **irrevocable**, world-wide license to publish, distribute, copy, exhibit and perform the work, in whole or in part, to authorize others to do so, to reproduce the published/electronic form of the contribution, and to prepare derivative works including, but not limited to, abstracts, lectures, lecture notes, press releases, reviews, text-books , reprint books, and translations.

AUTHORIZED REPRESENTATIVE

 5/30/97
(Signature) (Date)

Mary Sue O'Brien

Logistics & Technical Information Division

JET PROPULSION LABORATORY
CALIFORNIA INSTITUTE OF TECHNOLOGY

DETC97/VIB-4242

BENEFITS OF MODEL UPDATING: A CASE STUDY USING THE MICRO-PRECISION INTERFEROMETER TESTBED

Sanjay S. Joshi¹, James W. Melody², Gregory W. Neat³, and Andrew Kissil⁴

Jet Propulsion Laboratory
California Institute of Technology
Pasadena, California 91109

ABSTRACT

This paper presents a case study on the benefits of model updating using the **Micro-Precision Interferometer (MPI)** testbed, a full-scale model of a future spaceborne optical interferometer located at JPL. The MPI testbed is composed of several active and passive **optical** elements distributed across a **7 m x 7 m x 6.5 m** truss structure. Successful operation of this complex **opto-mechanical** system requires positional stabilities of these optical elements down to the ten-nanometer level. Design of such systems for space requires a disturbance modeling capability that integrates optical modeling, structural modeling and control system design. An integrated model of MPI was built in parallel with the testbed, enabling a unique model updating and validation opportunity. Physical parameters of the structural finite element model were updated based on two separate modal tests: a comprehensive **modal** test of the base structure alone and an **in situ** component modal test. This paper quantifies the effect of these physical parameter updates on **MPI** integrated model prediction **capability**. Specifically, the paper compares three sets of disturbance-input to optical-output transfer functions: (1) measured data from the testbed, (2) predictions from a **high-fidelity** model without any parameter updates, and (3) similar predictions for the model with updated physical parameters. **Results** from this study indicate that physical parameter updating has provided little benefit for disturbance modeling on the MPI test bed. These results will have significant impact on the modeling strategy adopted for the Spaceborne Interferometer Mission (SIM).

INTRODUCTION

The Spaceborne Optical **Interferometry Mission (SIM)**, a NASA mission planned for launch in the year **2003**, will **place** a 10-meter class optical interferometer into space. This instrument will use a partial aperture approach to make **astrometric** measurements and image celestial objects on the order of 4 times more resolution than can be achieved today with **Hubble** Space Telescope. The SIM instrument consists of hundreds of optical elements distributed across a flexible space structure. In order for the interferometer to be operational, optical elements must maintain positional stability to within 10 nanometers RMS.

The charter for the Jet Propulsion Laboratory Interferometer Technology Program is to mitigate risk for this optical-interferometer mission class (1). A number of ongoing complementary activities address these challenges including: integrated modeling methodology development and validation, hardware metrology testbeds, hardware vibration testbeds, and flight qualification of the **interferometer** components. Though all of these activities are necessary to buy down mission risk, it is integrated modeling that ultimately **will** be used in the mission and instrument design. Specifically, modeling will enable definition and flow down of spacecraft/instrument requirements, performance of spacecraft/instrument design trades, and prediction of instrument performance in the anticipated on-orbit disturbance environment.

In anticipation of these modeling needs, the Integrated Modeling of Optical Systems (IMOS) and the Controlled Optics Modeling Package (COM P) software packages were developed at JPL (2; 3). These packages enable an integrated modeling methodology that combines structural

¹ Corresponding author: Dr. Sanjay S. Joshi, Mail Stop 198-326,
Phone: (818) 565-8634, Email: sanjay.s.joshi@jpl.nasa.gov.

² Email: jmelody@csi.jpl.nasa.gov

³ Email: neat@huey.jpl.nasa.gov

⁴ Email: Andre.w.Kissil@cc2mhb.jpl.nasa.gov

modeling, optical modeling, and control system design within a common software environment.

The MPI testbed is a ground-based, suspended hardware model of a future space-based interferometer located at JPL (4; 5; 6; 7). The primary objective of the testbed is integration of the vibration attenuation technologies required to demonstrate the end-to-end operation of a space-based interferometer. Figure 1 shows a bird's-eye view of the testbed which contains all systems necessary to perform a space-based, optical interferometry measurement. These systems include a 7 m x 7 m x 6.5 m softly suspended truss structure with mounting plates for subsystem hardware, a six-axis vibration isolation system which supports a reaction wheel assembly to provide a flight-like input disturbance source, a complete Michelson interferometer with high-bandwidth optical control systems, internal and external metrology systems, and a star simulator that injects the "stellar" signal into the interferometer collecting apertures.

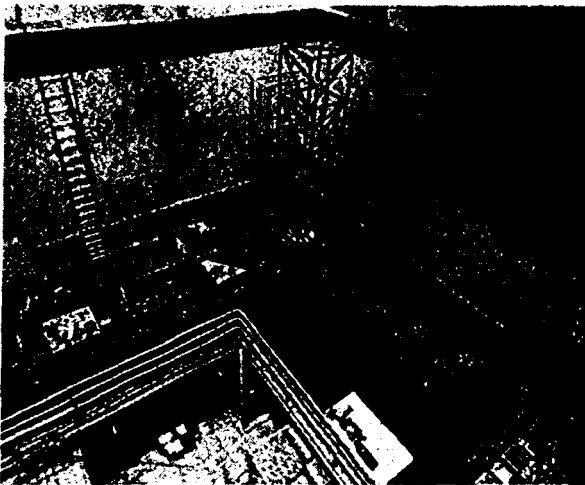


Figure 1. Bird's-eye view of the MPI Testbed.

A number of IMOS models of MPI were developed in parallel with the testbed which provided a unique opportunity to answer critical issues related to modeling complex opto-mechanical systems. These issues include:

- validation of the IMOS modeling methodology,
- application of model parameter updating techniques,
- assessment of the benefits of model parameter updating, and
- assessment of the benefits of high fidelity models.

Each MPI model in the suite of models differs in terms of structural model fidelity, whether the structural parameters were updated using modal testing, optical model fi-

delity, and/or control system model fidelity. To validate the IMOS modeling methodology, the approach was to use a high fidelity structural model, updated structural parameters, a high fidelity optical model and a high fidelity control system model (when appropriate). In the suite of MPI models, this model is the "best" representation of the testbed. References (8; 9) present IMOS modeling methodology results using this model.

The physical structural parameters were updated in the "best" model using two updating schemes. The first update involved estimating the physical parameters of the beams that make up the truss using data from a full-scale bare structure modal test (10; 11). The second update involved geometry modifications and parameter estimation of the component structures using data from an in situ component modal test (12).

To date, model updating was thought to be essential to achieving the "best" model prediction accuracy (13). This paper assesses the benefits of these parameter updates. This is done by creating a new MPI IMOS model which has the same fidelity as the "best" model but without the parameter updates. To quantify the improvement in prediction accuracy due to the parameter updates, the same disturbance transfer function was compared from three sources: (1) the "best" model, (2) the un-updated "best" model, and (3) the measured data from the hardware testbed.

For this case study, the measured data represents the "truth" so each model prediction is compared to this data. Results from studies such as this will help guide the modeling approach adopted for future complex opto-mechanical systems such as the Spaceborne Optical Interferometer Mission (SIM). If parameter updating provides significant improvement to model prediction accuracy, the additional time and costs associated with modal testing will be incorporated in the evolution of the flight hardware. If parameter estimates appear to provide little to the improvement of performance prediction accuracy, these steps may be eliminated.

The following sections describe the integrated modeling approach, the form of the MPIIMOS models used in this validation study, an overview of the previously performed updating procedures, the method of comparison, and the results of the comparison.

INTEGRATED MODELING

Integrated modeling is performed with two software packages: Integrated Modeling of Optical Systems (IMOS) (2) and the Controlled Optics Modeling Package (COMP) (3). Both packages have been developed at the Jet Propulsion Laboratory. IMOS is a set of functions that run within the Matlab environment (14), whereas COMP is

a stand-alone, FORTRAN-compiled program. A commercial version of COMP is available under the name **MACOS** (Modeling and Analysis of Controlled Optical Systems).

IMOS is a collection of **Matlab m-files** that can be used to perform structural finite element modeling and analysis, optical ray tracing, and thermal analysis. **IMOS** also provides graphics functionality that enables viewing of structural geometries, structural deformations, optical ray traces, and optical element prescriptions. The core files are easily coupled in **Matlab**, and can be extended by the user. **Matlab** toolboxes for control system design and analysis, signal processing, and optimization are available for enhancing the capability of **IMOS**. Detailed optical and thermal analysis are accommodated in IMOS by interfaces with COMP, and TRASYS and **SINDA** (for thermal analysis). The interface with COMP has been made effortless by creating a **Matlab mex-file** version of MACOS. The result is an extremely flexible tool that enables the user to integrate models from different disciplines and conduct analysis, design, and optimization trades that would otherwise be exceedingly difficult (2).

COMP is an optical analysis and modeling program, providing geometric ray-trace, differential ray-trace, and diffraction modeling capability. COMP concentrates on providing detailed optical models for integrated design and analysis tasks. In particular, the differential ray trace capability of COMP can be used to generate linear perturbation models of optical systems (3).

MPI INTEGRATED MODEL

The MPI integrated model form consists of a structural finite element model and a linear optical model that are integrated together. The structural model is generated with **IMOS**, whereas both IMOS and COMP are used to create the optical model. The integration and analysis are performed in **Matlab** with the aid of **IMOS** functions.

Structural Model

The structural model is specified in **IMOS** as a finite element geometry, shown in Figure 2. This geometry consists of plate, beam, truss, and rigid body elements, modeling the base truss structure and the components. The base truss structure is made up of three booms: the horizontal optics boom, the vertical tower, and the canted metrology boom. The components consist of inboard and outboard optics plates, a disturbance mount plate, two siderostat mounts, an optics cart containing an active delay line, the optics cart support structure, a hexapod isolation system, a passive delay line, and an external metrology beam launcher plate. The finite element model uses 2,577 degrees of free-

dom (**dof**) of which 1,832 dofs are independent with respect to the multi-point constraints (**MPCs**) of the rigid body elements (**RBEs**) (2). From the finite element geometry and

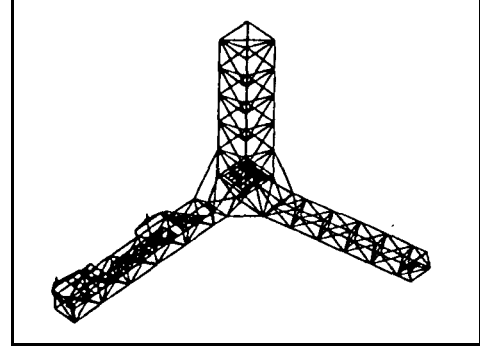


Figure 2. MPI Finite Element Geometry (compare with Figure 1).

its associated properties, the system mass and stiffness matrices are built. The result is a second-order, state-space description of the form:

$$M\ddot{d} + Kd = B_f \mathcal{F} \quad (1)$$

where M and K are the system mass and stiffness matrices, d is the nodal state, \mathcal{F} is a vector of force input, and B_f is the force influence matrix.

After the system mass and stiffness matrices are built, multi-point constraints are generated using RBE elements. These constraints take the form of (2):

$$d = \begin{bmatrix} d_n \\ d_m \end{bmatrix} = \begin{bmatrix} I_n \\ G_m \end{bmatrix} d_n = Gd_n \quad (2)$$

where d_n are the independent degrees of freedom and d_m are the dependent degrees of freedom. These constraints are then applied to Equation 1, reducing the state of the system to the independent degrees of freedom:

$$G^T M G \ddot{d}_n + G^T K G d_n = G^T B_f f \\ M_{nn} \ddot{d}_n + K_{nn} d_n = B_{n,f} \mathcal{F} \quad (3)$$

The **eigensolution** of Equation 3 is found, yielding flexible-body modes and **modeshapes**. The resultant **diagonalized** system is:

$$\ddot{\eta} + 2Z\Omega\dot{\eta} + \Omega^2\eta = \Phi_n^T B_{n,f} f \\ d = G\Phi_n\eta \quad (4)$$

where η is the modal state vector, Z is a diagonal modal damping matrix, Ω is the diagonal modal frequency matrix, and Φ_n is the eigenvector matrix. Z is formed by assuming a modal damping of 0.3% for all global flexible-body modes.

Optical Model

The optical model begins with a specification of the optical prescription. This prescription includes the shapes, positions, and orientations of the optical elements. A ray trace of the optical prescription is shown in Figure 3. This optical prescription is generated in IMOS based on the prescription of the actual optical elements of MPI (see Figure 4). The model generation uses the structural finite element geometry in order to simplify the prescription definition and to ease the succeeding structural-optical model integration. This allows the location of the actual optical elements to be measured with respect to reference points on the structure as opposed to with each other. Furthermore, structural nodes that correspond to optical element attachment points are easily identified or defined.

Once the optical prescriptions are specified, they are exported to COMP, where linear optical models are created. These linear models are calculated by performing an analytic differential ray trace (3). The result is a model of the form:

$$y = C_{opt}d \quad (5)$$

where d is a vector of optical element position and orientation perturbations, y is a vector of optical output, and C_{opt} is the optical sensitivity matrix. The optical output can be pathlength, wavefront tilt, or spot motion.

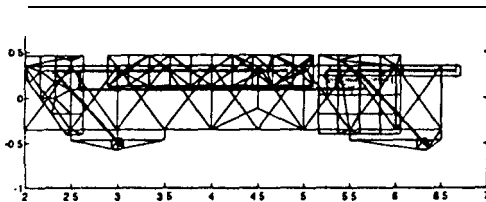


Figure 3. Ray trace of the MPI optical prescription on the finite element geometry of the optics boom.

Structural-Optical Model Integration

Once the structural modal model and the linear optical model have been created, they are integrated to form a structural-optical model. This integrated model is specified



Figure 4. Actual optical layout on the MPI optics boom.

in first-order, state-space form, lending itself most easily to analysis with existing Matlab functions. In particular, the state-space integrated model can be used for frequency-domain analysis, time-domain simulation, and closed-loop synthesis.

First, the structural model is truncated to remove modes above the bandwidth of expected disturbances (i. e., above 900 Hz) (15; 16). The truncated modal model is then converted into first-order, state-space form by using the substitution (2):

$$x = \begin{bmatrix} \eta_k \\ \dot{\eta}_k \end{bmatrix} \quad (6)$$

Resulting in:

$$\begin{aligned} \dot{x} &= Ax + Bf \\ d &= C_d x + Df \end{aligned} \quad (7)$$

with:

$$\begin{aligned} A &= \begin{bmatrix} 0 & I \\ -2Z_k \Omega_k & -\Omega_k^2 \end{bmatrix} & B &= \begin{bmatrix} 0 \\ \Phi_{nk}^T G^T B_f \end{bmatrix} \\ C_d &= \begin{bmatrix} G \Phi_{nk} & 0 \\ 0 & G \Phi_{nk} \end{bmatrix} & D &= 0 \end{aligned} \quad (8)$$

where the subscript k refers to the set of kept modeshapes.

Finally, the linear optical model is incorporated into the first-order model. The optical output is obtained by premultiplying d by the optical sensitivity matrix, C_{opt} . In this case the matrix C of the measurement equation of Equation 7 becomes:

$$C = C_{opt} C_d \quad (9)$$

Note that the matrix D of Equation 7 is still zero but now has different dimension.

PHYSICAL PARAMETER UPDATES

Two sets of physical parameters were used in this study which led to two **MPI** models: (1) one in which the parameters were derived based on engineering judgement and knowledge of the testbed geometry (un-updated "best" model), and (2) one in which the parameters were derived using two parameter updating procedures based on measured data (updated "best" model). This section provides an overview of the parameter estimation methods used.

As described in (17), methods used to update finite element models from measured test data can be described as global or local. Global methods directly modify the coefficients of the mass and stiffness of the finite element model. Local methods modify physical parameters, such as element geometric and material properties. Because of the phased assembly and development of the **MPI** testbed, any model updating would be useless unless it allowed for incorporation of added components. For this reason, local model updating **was** used on the **MPI** structure. This was done in two phases, corresponding to the phased delivery of the **MPI** testbed. The first phase updated the base truss structure and the second phase focused on added structural components.

Bare-Truss Parameter Updates This procedure used measured mode shapes and frequencies along with a Bayesian estimation technique to update physical parameters of the bare structure elements (18). Measurements came from two independent modal tests performed on the bare structure prior to the addition of any components (18). The Bayesian technique used was that reported in (19) and (20). This technique establishes updated physical parameters by minimizing a cost functional that is based on both errors in measured and predicted eigenproperties and in variation of physical properties from their original estimates. As reported in (18) for the **MPI** case, the optimization problem becomes

$$\min ([S_{uu} (u^* - u_p)] , (u_m - u_p)] + [S_{rr} (r_o - r), (r_o \cdot r)]) \quad (10)$$

In this equation, $[\cdot, \cdot]$ is a valid inner product, u_m is the vector of measured eigenproperties, u_p is the vector of model predicted eigenproperties, r is the vector of physical parameters to be estimated, with r_o as the original estimate. The weighting coefficients S_{uu} and S_{rr} are the covariance estimates of the physical parameters and eigenproperties, respectively. The Bayesian estimation algorithm was implemented in **NASTRAN** on a Cray supercomputer. This allowed simultaneous estimation of the geometric properties (A, I, and J) and material properties (ρ) of each beam element of the bare-truss structure (11).

Component Parameter Updates After updating the bare truss elements, the next phase involved identifying parameters of the components that were attached to the base structure (21). These included optics plates, an active delay line, siderostat mounts, and a payload plate. Due to a tight hardware delivery schedule and limitations *on test* hardware, individual component tests were not performed. Rather, an *in situ* component test/ID method was employed in which the components were tested while attached to the main structure. Thus the component response could not be isolated from that of the main structure.

In situ component tests are conducted in an identical manner as a standard modal test using FRF measurements. Accelerometers are distributed throughout the main structure and the components, and multiple excitation locations can be used. In the *in situ* component test, the modes that are identified are those of the coupled structure/component system. In the component model updating phase, it was assumed that the finite element parameters of the base structure were correct, and that only the parameters of the components were in error.

An element modal strain energy error (EMSEE) analysis provided element error localization (12). The EMSEE allowed systematic quantification of the element parameter errors. Evaluation of the EMSEE for the identified mode shapes resulted in the discovery of several model form errors, both human errors and insufficient fidelity in certain elements. The correction of these terms resulted in significant improvement in the model accuracy. Finally, EMSEE was used to target parameters for estimation.

Model parameters estimation provided for update of physical parameters of components as they were added on, preserving the validity of the previously updated base structure. Similar to the bare-truss update, a **Bayesian** estimation technique was used to estimate component parameters. As opposed to the bare-truss parameter estimation, this estimation was implemented in **IMOS** on a Sun workstation. In order to ease the computational burden, the algorithm incorporated a component mode synthesis solution of the **eigenvalue** problem, thereby taking advantage the fact that only a portion of the model was effected by the estimated physical parameter (13).

Unlike the bare-truss model update, the *in situ* update was not performed comprehensively. In fact, only a **single** parameter from one component was estimated. This parameter was targeted by the EMSEE as particularly in error.

COMPARISON METHOD

Approach

Interferometer performance is primarily degraded by variation in optical pathlength difference (OPD), i.e., the difference in the distances that the light travels from the stellar source, through each arm of the interferometer to the interference optical detector. This difference must be stabilized to the 10 nm (RMS) level in the on-orbit mechanical disturbance environment (22). It is expected that the dominant on-orbit disturbance will be the high frequency harmonics from the reaction wheel assemblies that result from bearing imperfections, wheel imbalances, etc.

In contrast to estimating modal characteristics as in (12; 21), disturbance input (at the reaction wheel location) to stellar OPD output transfer functions are the important measurement since they completely characterize (in a linear sense) the propagation of disturbances to OPD. Therefore, in this study, these disturbance transfer functions were predicted with the updated “best” and un-updated “best” models and compared with measured disturbance transfer functions from the testbed.

MPI Measurement

Figure 5 shows the disturbance input location relative to the OPD output location for the MPI testbed. This disturbance transfer function was measured for three force disturbance directions: (x, y, z). An HP data analyzer was used to collect the data. A 10 N shaker, mounted at the base of the tower, applied the force input in each of the three directions. The force input was measured with a load cell mounted between the shaker and the structure. The analyzer calculated the transfer function from force input to OPD output.

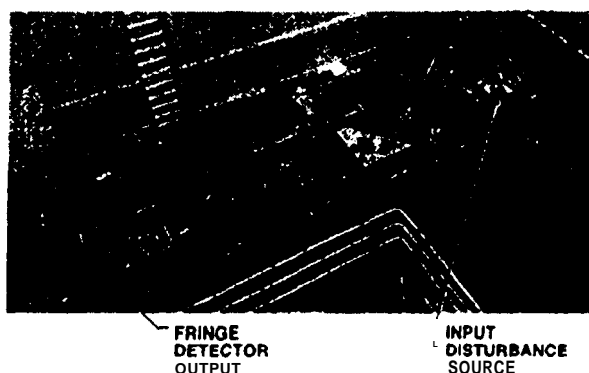


Figure 5. Locations of disturbance input and OPD output on the MPI testbed.

Comparison Metric

In general on space-based interferometers, mechanical disturbances will be either broadband or narrowband with the energy varying over broad frequency ranges as a function of time (15; 16). In either case, the power spectral density of the disturbance is broadband. Therefore, the integrated model should be accurate in a broadband sense. More specifically, we desire σ_{opd} to be accurate, where (23):

$$\sigma_{opd}^2 = \frac{1}{\pi} \int_0^{\infty} |G(j\omega)|^2 \Phi_d(\omega) d\omega \quad (11)$$

for a broadband disturbance power spectral density, $\Phi_d(\omega)$, and a disturbance to OPD transfer function, $G(j\omega)$.

Since Equation 11 yields the quantity that we wish to accurately predict, we can use this same equation as a metric to characterize the measured and predicted transfer functions. As opposed to picking a particular expected disturbance power spectral density, **bandlimited** white noise (over $[\omega_{min}, \omega_{max}]$) is used:

$$\sigma_g^2 = \frac{A_d}{\pi} \int_{\omega_{min}}^{\omega_{max}} |G(j\omega)|^2 d\omega \quad (12)$$

where A_d is the amplitude of the **bandlimited** white noise disturbance power spectral density with ω_{min} and ω_{max} defining the frequency range of interest. σ_g is used instead of σ_{opd} in order to stress that the result is a metric of the transfer function itself.

Using this metric, the accuracy of the model can be quantified by comparing σ_g for the **un-updated** predicted, updated predicted, and measured transfer functions. As such, the particular value of the disturbance amplitude is immaterial. The amplitude is chosen so that the variance of the disturbance is one. This choice is arbitrary, and the value of σ_g has no significance by itself. It is the **comparison** of the metrics for corresponding measured and predicted transfer functions that is meaningful.

RESULTS

The modulus of the measured transfer functions, along with the corresponding predicted transfer functions, are shown in Figures 6-8. The predicted transfer functions were calculated by applying standard **Matlab** functions to the integrated model with disturbance force input and OPD output. The value of the broadband metric, also calculated with **Matlab** functions, is given in the legend for each transfer function.

The results of σ_g comparisons are shown in Table 1. The bandwidth of interest is [4, 900] Hz. Below 4 Hz the

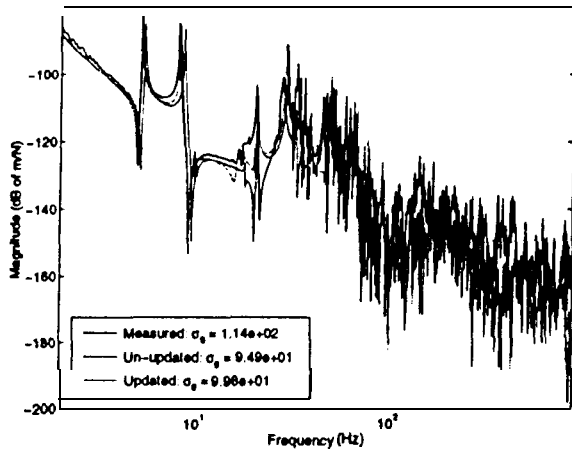


Figure 6. Predicted and measured MPI disturbance to OPD transfer function: x-axis force input.

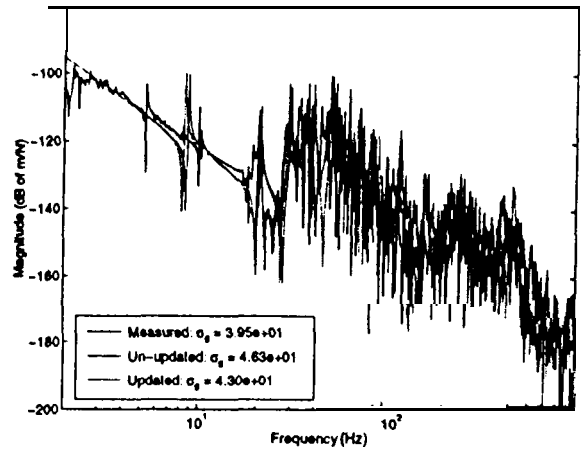


Figure 8. Predicted and measured MPI disturbance to OPD transfer function: z-axis force input.

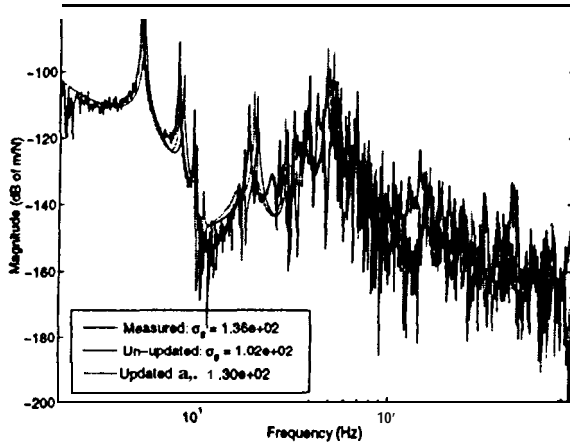


Figure 7. Predicted and measured MPI disturbance to OPD transfer function: y-axis force input.

force capability of the shaker is limited and the testbed suspension modes pollute the measurement. Above 900 Hz the mechanical disturbances are expected to have no energy. This bandwidth is further broken roughly into decades and comparisons are shown for these “decades.” Units are not given in the table so as to discourage the reader from attaching significance to the separate values. *The disturbance transfer function magnitude plots as well as the table show that the parameter updating did not have an appreciable effect in this case study.*

CONCLUSIONS AND FUTURE WORK

This paper presented a case study on the benefits of model updating using the JPL Micro-Precision Interferom-

Disturbance input		σ_g			
		4-1 OH,	10 - 100 Hz	100 - 900 H,	1 - 900 Hz
x-axis Force	meas	997	541	70	1,197
	un-updated factor	706	634	32	949
	updated factor	0.71	1.17	0.47	0.83
y-axis Force	meas	764	641	25	998
	un-updated factor	0.77	1.18	0.36	0.88
	updated factor	1,313	360	69	1,369
z-axis Force	meas	946	379	31	1,020
	un-updated factor	0.72	1.05	0.45	0.75
	updated factor	1,053	768	20	1,304
z-axis Force	meas	0.80	2.13	0.29	0.96
	un-updated factor	185	346	50	395
	updated factor	0.97	1.21	1.60	1.17
z-axis Force	meas	184	383	64	490
	un-updated factor	0.99	1.11	1.29	1.09
	updated factor				

Table 1. Broadband transfer function metric comparison between the predicted and measured transfer functions of the MPI Testbed.

eter (MPI). The paper quantitatively compared three data sets to perform this evaluation: (1) actual test data from the test article, (2) model predictions from a high-fidelity model of the test article without any parameter updates, and (3) a high-fidelity model of the test article with param-

eter updates based on modal test data. It was shown that parameter updating did not have an appreciable effect in this case study.

This result is influenced by both choice of comparison metric and method of updating. Before declaring parameter updating useless, several further investigations should be carried out. As mentioned earlier, in this case study, bare truss physical parameters were thoroughly updated. However, only a single component parameter was updated using in-situ test data. If all component parameters were updated, a greater benefit may be realized. Secondly, other parameter updating techniques may also yield more positive results. Ongoing work focuses on addressing these areas.

ACKNOWLEDGEMENTS

This work was performed at the Jet Propulsion Laboratory, California Institute of Technology, under contract with the National Aeronautics and Space Administration.

REFERENCES

- R. A. Laskin, "Technology for space optical interferometry," in *Proc. 33rd Aerospace Sciences Meeting and Exhibit*, vol. 95-0825, (Reno, NV), AIAA, Jan. 1995.
- M. H. Milman, H. C. Briggs, W. Ledebuer, J. W. Melody, R. L. Norton, and L. Needels, *Integrated Modeling of Optical Systems User's Manual, Release 2.0*, Nov. 1995. JPL D-130.10 (JPL Internal Document).
- D. Redding, *Controlled Optics Modelling Package User Manual, Release 1.0*, June 1992. JPL D-9816 (JPL Internal Document).
- G. W. Neat, L. F. Sword, B. E. Hines, and R. J. Calvet, "Micro-precision interferometer testbed: End-to-end system integration of control structure interaction technologies," in *Spaceborne Interferometry* (R. D. Reasenberg, ed.), vol. 1947 of *Proc. SPIE*, (Orlando, FL), pp. 91-103, Apr. 1993.
- B. E. Hines, "Optical design issues for the micro-precision interferometer testbed for space-based interferometry," in *Spaceborne Interferometry* (R. D. Reasenberg, ed.), vol. 1947 of *Proc. SPIE*, (Orlando, FL), pp. 114-125, Apr. 1993.
- G. W. Neat, J. F. O'Brien, N. M. Nerheim, R. J. Calvet, H. Singh, and S. Shaklan, "Micro-precision interferometer testbed: First stabilized stellar fringes," in *Spaceborne Interferometry II* (R. D. Reasenberg, ed.), vol. 2447 of *Proc. SPIE*, (Orlando, FL), pp. 104-115, Apr. 1995.
- G. W. Neat, A. Abramovici, J. W. Melody, R. J. Calvet, N. M. Nerheim, and J. F. O'Brien, "Control technology readiness for spaceborne optical interferometer missions," in *Proc. Space Microdynamics and Accurate Control Symposium*, (Toulouse, France), May 1997.
- J. W. Melody and G. W. Neat, "Integrated modeling methodology validation using the micro-precision interferometer testbed," in *Proc. 35th IEEE Conference on Decision and Control*, vol. 4, (Kobe, Japan), pp. 4222-4227, Dec. 1996.
- J. W. Melody and G. W. Neat, "Integrated modeling methodology validation using the micro-precision interferometer testbed: Assessment of closed-loop performance prediction capability," in *Proc. American Control Conference*, (Albuquerque, NM), June 1997.
- T. G. Came, R. L. Mayes, and M. B. Levine-West, "A modal test of a space-truss for structural parameter identification," in *Proc. 11th IMAC*, (Kissimmee, FL), Feb. 1993.
- J. R. Red-Horse, E. L. Marek, and M. B. Levine-West, "System identification of the jpl micro-precision interferometer truss: Test-analysis reconciliation," in *Proc. 34th SDM*, (La Jolla, CA), Apr. 1993.
- M. B. Levine-West and J. W. Melody, "Model updating of evolutionary structures," in *Proc. 15th ASME Biennial Conference on Mechanical Vibration and Noise*, (Boston, MA), Sept. 1995.
- M. B. Levine, M. H. Milman, and J. W. Melody, "Experimental verification of integrated opto-structural model predictions," in *Proc. Space Microdynamics and Accurate Control Symposium*, (Toulouse, France), May 1997.
- The Math Works Inc., *Matlab User's Guide*, Aug. 1992.
- J. W. Melody and H. C. Briggs, "Analysis of structural and optical interactions of the precision optical interferometer in space (POINTS)," in *Spaceborne Interferometry* (R. D. Reasenberg, ed.), vol. 1947 of *Proc. SPIE*, (Orlando, FL), pp. 44-57, Apr. 1993.
- S. Shaklan, J. Yu, and H. C. Briggs, "Integrated structural and optical modeling of the orbiting stellar interferometer," in *Space Astronomical Telescope and Instrument II*, *Proc. SPIE*, (Orlando, FL), Apr. 1993.
- N. Roy, A. Girard, L. Bugeat, and J. Bricout, "A survey of finite element updating methods," in *Proc. International Symposium on Environmental Testing for Space Programs- Test Facilities and Methods*, (Noordwijk, The Netherlands), June 1990.
- M. B. Levine-West, J. R. Red-Horse, and E. L. Marek, "A systems approach to high fidelity modeling," in *Proc. 1st International Symposium on Microdynamics and Accurate Control*, (Nice, France), Nov. 1992.
- J. D. Collins, G. C. Hart, T. K. Hasselman, and B. Kennedy, "Statistical identification of structures," *AIAA Journal*, pp. 185-190, Feb. 1974.
- T. K. Hasselman, J. D. Chrostowski, and T. J. Ross, "SSID/PDAC theoretical manual (version 1.0)," Technical Report TR-91-1 152-1, Engineering Mechanics Associates, Dec. 1991.
- J. W. Melody and M. B. Levine-West, "High fidelity modeling of evolutionary structures in IMOS," in *Proc. First World Conference on Structural Control*, (Los Angeles, CA), pp. WP1-98 to WP1-107, Aug. 1994.
- M. Shao and D. M. Wolff, "Orbiting stellar interferometer," in *Spaceborne Interferometry II* (R. D. Reasenberg, ed.), vol. 2447 of *Proc. SPIE*, (Orlando, FL), pp. 228-239, Apr. 1995.
- A. Papoulis, *Probability, Random Variables, and Stochastic Processes*. New York: McGraw-Hill, 3rd ed., 1991.